Strength and stability of active ligand-receptor bonds: A microtubule attached to a wall by molecular motor tethers

Dipanwita Ghanti, Raymond W. Friddle, and Debashish Chowdhury

Phys. Rev. E **98**, 042415 — Published 26 October 2018

DOI: 10.1103/PhysRevE.98.042415

Strength and stability of active ligand-receptor bonds: a microtubule attached to a wall by molecular motor tethers

Dipanwita Ghanti,[1] Raymond W. Friddle,[2] and Debashish Chowdhury[1]

[1] *Department of Physics, Indian Institute of Technology, Kanpur 208016, India*
[2] *Sandia National Laboratories, Livermore, CA 94550, USA*

We develop a stochastic kinetic model of a pre-formed attachment of a microtubule (MT) with a cell cortex, in which the MT is tethered to the cell by a group of active motor proteins. Such an attachment is a particularly unique case of ligand-receptor bonds: The MT ligand changes its length (and thus binding sites) with time by polymerization-depolymerization kinetics, while multiple motor receptors tend to walk actively along the MT length. These processes, combined with force-mediated unbinding of the motors, result in an elaborate behavior of the MT connection to the cell cortex. **A fundamental challenge in this context is to understand how such a pre-formed attachment maintains its integrity long enough in spite of the ongoing turnover of the MT subunits from its depolymerizing plus end and withstands potentially disruptive effects arising from enhanced rates of detachment of the tethering motors because of external tensions.** We present results for the strength and lifetime of the system through the well-established force-clamp and force-ramp protocols when external tension is applied to the MT. The simulation results reveal that the MT-cell attachment behaves as a catch-bond or slip-bond depending on system parameters. We provide analytical approximations of the lifetime and discuss implications of our results on in-vitro experiments.

Correspondence: debch@iitk.ac.in , rwfridd@sandia.gov

I. INTRODUCTION

In eukaryotic cells, sister chromatids are segregated by a complex multi-component machine known as the mitotic spindle [1–3]. During the morphogenesis of the spindle [4, 5], microtubules (MT) play a critical part as dynamic tethers between the centrosomes and other major components of the cell, such as the cell cortex and the kinetochores [6, 7]. As such, the biophysical properties of MTs have attracted investigation recently[8, 9] due to their indispensable role in the timely and accurate segregation of chromosomes — a process essential to cell survival.

Understanding the adhesion physics of a single astral MT with the cortex is the first step in ultimately understanding how intracellular forces collectively determine the position and orientation of the spindle [10–15]. The theory of oscillations of the mitotic spindle, arising effectively from the collective dynamics of all the astral MTs tethered to the cortex by attaching/detaching motors, has been reported earlier [16, 17]. Here we consider the behavior of a single MT-cortex connection, which is amenable to experimental investigation by way of (single-) molecule force spectroscopy (MFS) [18].

The MT-cortex interaction is viewed as an analog of a 'ligand-receptor bond' [19, 20] where the end of the MT filament (ligand) adheres to the specific binding partners (receptor) that link it with the cortex. However, unlike common ligands, a MT exhibits unique polymerization-depolymerization kinetics [21]. Furthermore, the corresponding receptor proteins are 'active' in the sense that they consume chemical fuel for their mechanical function.

The transient molecular joints formed by the plus ends of MTs with the kinetochores and cell cortex must survive long enough so that the function of the mitotic spindle is not disrupted by premature rupture of these attachments. How the integrity of these attachments are maintained in spite of the ongoing turnover of the MT subunits from its depolymerizing plus ends is itself a challenging question. Moreover, the molecular joints should be able to withstand the potentially disruptive effects of tensions exerted by other components of the spindle. In the specific case of the MT-cortex attachments, the unbinding of the motor heads from the MT during each of their ATPase cycles can further hasten the rupture of the attachment unless compensated by fresh binding of other motors, or rapid rebinding of the same motor, to the MT.

The aim of this paper is to develop a minimal mathematical model of an attachment formed by a single astral MT with the cell cortex by capturing the essential roles of only the key components identified experimentally till now. In spite of the simplicity of the system, our analysis reveals the cooperative effects of multiple motors that give rise to the emergent collective properties of the attachment. Such collective phenomena are of general interest in several branches of physics and biology [22–27]. These theoretical predictions can, in principle, be tested by corresponding single-molecule experiments *in-vitro* [28].

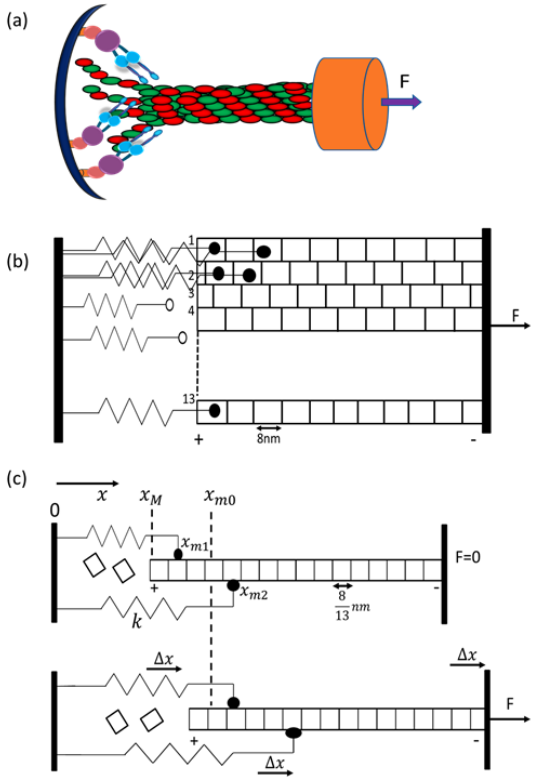

FIG. 1. (a) In the cartoon of a MT-cortex attachment formed by dyneins, each dynein is permanently attached to the cell cortex by a spring-like elastic element. External Force F is applied on the orange cylinder from which MTs are generated. (b) The 3D cylindrical MT is 'unwrapped' into a 2D sheet consisting of 13 mutually parallel protofilaments each of which consists of identical subunits of length 8nm and can bind with the cortical dyneins. (c) The 2D sheet of (b) is 'projected' onto an effectively 1D model in which the effective dimer size becomes 8/13 nm (the relative sizes of the dimers in (b) and the effective dimers in (c) are not drawn to scale). But, as the step size of a dynein motor is 8 nm, a motor's head can hop to the next $\delta = 13^{\text{th}}$ site on this 1D model. x_M represents the distance of MT tip from wall. The mid-points of the pair of heads of two distinct motors are shown at distances x_{m1} and x_{m2} from the wall. The spring constant of the elastic element connecting a motor with the cortex is k and its rest length is x_{m0} while Δx denotes the extension of the spring caused by the external force F.

II. MODEL AND METHOD

A. The model

Microtubules are cylindrical hollow tubes of approximately 25 nm diameter, nominally assembled from 13 parallel protofilaments. Each protofilament is assembled by globular protein hetero-dimers consisting of α and β tubulins. The length of each α-β dimer is about 8 nm. The MT is a polar filament distinguished by a plus end, which is linked to the cell cortex by dynein motor proteins and a minus end anchored in the centrosome [29]. Dynein are motors that specifically bind to equispaced binding sites on the surface of a MT, with a tendency to actively walk towards the minus end of the MT [23, 24].

A cartoon of a MT-cortex attachment formed by cortical dyneins with a single MT is drawn in Fig.1(a). To reduce the full 3D system to an effective 1D model, we first imagine splitting the cylindrical tubule open into a two-dimensional sheet, as depicted schematically in Fig.1(b). In this 2D representation, the 13 protofilaments of the MT are arranged side-by-side parallel to each other. We then project the two-dimensional sheet onto a line resulting in a strictly one-dimensional lattice with the lattice constant 8/13 nm (shown in Fig.1(c)) [30–34]. As with the dynein motor, the molecular motors in our model are minus-end directed. Since the step size of a dynein motor is 8 nm, on this 1D representation of the MT a motor's head can hop from the j-th site to the to the next $j+\delta$-th site where $\delta = 13$. We represent the cortex by a rigid wall which coincides with the origin of the 1D coordinate system. The X-axis is chosen to be perpendicular to the wall and +X direction is oriented towards right so that x increases from left to right. The plus end of the MT is oriented along the -X direction.

In what follows, we use the above one-dimensional model of the dynein-mediated MT-cortex attachment implementing conditions that mimic the protocols of MFS [35–38]. We assume a pre-formed attachment as the initial condition where all the motors are attached to randomly selected positions on the MT. In our MFS *in-silico*, we treat the two common experimental protocols: *force-clamp*, which measures the bond lifetime under constant tension, and *force ramp*, the force at which the bond ruptures under linearly increasing tension [19].

Each motor can either attach or detach from the MT, and walk in either direction along the MT. The tail of each dynein motor is an elastic element permanently anchored on the face of the rigid wall. Thus extension of a motor away from the wall is modeled as a Hookean spring of spring constant k and rest length x_{m0}. With respect to the origin, $x_{mi}(t)$ denotes the position of the *midpoint* of i^{th} molecular motor at time t while $x_M(t)$ denotes the corresponding position the MT tip (see Fig.1(c)).

Let N_d be the total number of dynein motors that can simultaneously attach to the MT whereas $n(t)$ denotes the number of motors attached at time t (i.e., $n(t) \leq N_d$). For an unbound motor, $\mathcal{K}_{on}$ denotes the rate of binding of its head to the MT. Therefore, the rate at which any unbound motor binds to the MT is [39]

$$k_{on}(n) = (N_d - n)\mathcal{K}_{on} \tag{1}$$

Applying a tensile force, F, to the MT minus-end will move all n motors by a distance Δx (Fig. 1(c)). The displacement of a motor caused by the external force and that due to the directed walking of the motor towards the minus end of the MT are both captured by x_{mi}. Thus, the force experienced by the i^{th} motor is given by the corresponding force of the elastic linkage at that exten-

sion,

$$F_i = k(x_{mi} - x_{m0}) \tag{2}$$

where x_{m0} is the rest length of the spring.

Following Kramers (or Bell) theory, [40, 41], we assume that the instantaneous rate of unbinding one of the n motors from the MT is approximately [39]

$$k_u(F_i, n) = nk_{u0}e^{|F_i|/F_d} \tag{3}$$

where k_{u0} denotes the rate of unbinding of a single motor in the absence of load force. The characteristic 'detachment force' F_d can be expressed as $F_d = k_BT/x_d$ where x_d is the distance from the energy minimum to maximum for the motor/MT interaction potential.

Similarly, the effective rate of forward stepping of a motor is given by

$$k_f(F_i) = k_{f0}e^{-F_i\gamma/F^\star_{sp}} \tag{4}$$

Based on experimental observations, we assume that a motor can also step towards the positive end of the MT [42–44]; thus we model stepping in the 'reverse' direction by

$$k_r(F_i) = k_{r0}e^{F_i(1-\gamma)/F^\star_{sp}} \tag{5}$$

where the constant parameter γ $(0 < \gamma < 1)$ is the fraction of the path ℓ over which work is done and the characteristic force $F^\star_{sp}$ can be expressed as k_BT/ℓ where ℓ is the length of a single MT subunit. The rate k_{r0} of stepping of a motor towards the plus end of the MT in the absence of load force is very small ($k_{r0} << k_{f0}$) because the natural direction of these motors is the minus end of MT.

The rates of polymerization and de-polymerization of a MT tip are given by α and β, respectively. The rate of depolymerization of MT is suppressed by externally applied tension [45]. We assume that the MT-bound minus-end directed motors at the tip (plus-end) of the MT prevents MT protofilaments from curling outwards, thereby slowing down or speeding up depolymerization rate depending upon the position of the MT tip [11]:

$$\beta = \beta_0 \exp\left(-\sum_{i=1}^{n} F_i(x_{mi})[H(x_{mi} - x_M) - H(x_{mi} - x_M - \delta l)]/F_\star\right) \tag{6}$$

where $F_\star$ is the characteristic load force at which the MT depolymerization rate is an exponentially small fraction of β_0. $H(x_{mi})$ is the standard Heaviside theta function which ensures that the force affects the depolymerization rate β only if the motor is bound between x_M and $x_M+\delta l$.

The overdamped Langevin equation that governs the kinetics of the MT in the aqueous medium has the standard form

$$\frac{dx_M(t)}{dt} = \frac{F - \sum_{i=1}^{n} F_i(x_{mi})}{\Gamma} + (\beta - \alpha)\ell + \frac{\eta(t)}{\Gamma} \tag{7}$$

where $\eta(t)$ is a Gaussian white noise, Γ is the effective viscous drag coefficient of the MT along with the motor and ℓ, the length of each subunit of MT is also the spacing between the successive motor-binding sites on the MT.

TABLE I. Numerical values of the parameters used in simulation

Parameter	Values
Spacing between binding sites on MT ℓ[46–48]	$\frac{8}{13}$ nm
Rate of MT polymerization α [46–49]	30 s^{-1}
Rate of load-free MT depolymerization β_0 [46–49]	350 s^{-1}
Rate of motor binding to MT k_{on} [50, 51]	1.6 s^{-1}
Rate of motor unbinding from MT k_{u0} [51, 52]	0.27 s^{-1}
Rate of motor forward stepping k_{f0} [50, 53]	81.25 s^{-1}
Rate of motor backward stepping k_{r0} [39]	9.0 s^{-1}
Characteristic depolymerization force $F_\star$	0.1 pN
Characteristic detachment force F_d [54]	0.67 pN
Characterstic spring force of motor $F^\star_{sp}$	1 pN
Rest length of elastic linkage x_{m0}	12.3nm
Linkage spring constant k	0.1pN/nm
Stepping parameter γ	0.5
Effective drag coefficient Γ [46–48, 55]	6pNs/μm

B. Simulation method

The simulations based on our theoretical model were carried out using the Gillespie algorithm [56]. In our simulation we discretized our system so that movement of the motor along with the motion of the MT is discrete. In each time step Δt, eight types of events are possible, namely, binding/ unbinding, forward/backward hopping of any motor, polymerization and depolymerization of MT tip and forward/backward movement of the whole MT body.

As stated before, initially, all the motors are attached to randomly selected positions on the MT. The MT tip is also placed adjacent to the wall. Rate constants are then determined based on each motor position. A motor can unbind from its occupied site with the unbinding rate given by eq.3. Similarly, a motor can jump forward or backward with the transition rates given by eq.4 and eq.5 respectively, provided the next δth site is empty. Finally, we assume that a depolymerization event, governed by

eq.6, can carry away a motor if it is concurrently located at the MT tip x_M.

At equilibrium, unbound motors are spatially distributed in 1D by the Boltzmann-weighted energy of their tethering springs:

$$P(x) = \sqrt{\frac{k}{2\pi k_B T}} \exp(-\frac{k(x - x_{m0})^2}{2k_B T}) \qquad (8)$$

This distribution will be truncated as the $x < 0$ is not allowed here and also dynamics of the MT will put constraint on the motor head as they only can bind to MT. In our simulation, we have used truncated normal distribution with $k = 0.1$ pN/nm the standard deviation of unbound motor fluctuations is only $\sigma = 12.3$ nm. That is, rarely would the spring naturally stretch more than $\pm 2\sigma = \pm 24.6$ nm. A suitable location for binding is drawn from the cumulative distribution $\int_{x_M}^{\infty} P(x)$ by inverse transform sampling, and checked if the chosen site is empty. In this way, the position for binding is selected.

By the equation of motion (7), the polymerization and depolymerization rates control x_M by changing the length of the MT with $x_M + \ell$ or $x_M - \ell$ discretely depending upon the events. But external forces influence movement of the whole MT by the resultant force acting on it, i.e. $F - \sum_{i=1}^{n} F_i(x_{mi})$. To treat movement of the whole MT within our discretized system, we define the corresponding rate constant by $w = \frac{F - \sum_{i=1}^{n} F_i(x_{mi})}{\Gamma \ell}$. The sign of the expression w decides the movement of MT in forward (positive) or backward (negative) directions.

The time evolution of the motor-MT attachment is monitored until, for the first time, all the motors are detached from the MT. This first passage time [57–60] is identified as the lifetime of the attachment for both the force clamp and force ramp conditions. We have generated trajectories of up to 10^6 time steps which were then averaged to arrive at the results of interest. The common parameter values used in the simulation are listed in table I.

We now summarize the simplifying assumptions made in formulating the model MT-cortex attachment:
(i) Although there are some indications that, occasionally, a dynein motor can step on to protofilaments on its left or right, we ignore such possibilities. Instead, we assume that, once attached to a particular protofilament, a dynein motor will step longitudinally only along that protofilament till it finally detaches thereby losing the memory of the protofilament on which it walked.
(ii) The elastic element that connects each individual dynein to the cortex is assumed to be a Hookean spring.
(iii) So far as the binding of unbound dynein motors to the MT is concerned, all the unbound motors are equally likely to bind, as expressed by eq.(1), while the actual location of binding of a motor is probabilistically decided by the eq.(8).
(iv) In principle, more than one dynein can walk along the same protofilament simultaneously. Since none of the dynein-binding sites can accommodate more than one dynein motor head at a time, in principle, the mutual exclusion of the motor heads should be taken into account while a motor tends to step along a protofilament. However, for simplicity, we do not check for such mutual exclusion in our model.
(v) We represent the cell cortex by a rigid wall; the mechanical softness of the cortex as well as its dynamic structure and molecular composition are ignored by this approximation.
(vi) Each MT that interacts with the cell cortex can, in principle, bend in such a way that a segment of its plus end can become approximately parallel to the cortex itself before curving away from it; for simplicity, we ignore such possibilities and assume the MT to remain perpendicular to the cortex.
(vii) In principle, diffusion of the actin layer in the cell cortex can dynamically alter the motor density; however, in our model, we do not consider any time dependence of the total number N_d of the dynein motors that can attach to the MT.
(viii) We assume that a depolymerization event carries away a motor if it is concurrently located at the MT tip. In principle, one can envisage an alternative scenario where a motor located at the MT tip can stay attached to the newly exposed tip, instead of getting carried away with the departing unit during depolymerization of the MT. The possible consequences of this alternative scenario may be explored in the future.

TABLE II. Values of all the coefficients of Eq.12 used in Fig.3(b)

$F_\star$ (pN)	a (s)	b (s)	c (s)
0.05	5.51×10^{-2}	1.57×10^{-3}	4.52×10^{-5}
0.2	6.55×10^{-2}	2.6×10^{-3}	9.23×10^{-5}
1	9.09×10^{-2}	5.5×10^{-3}	2.24×10^{-4}
10	8.94×10^{-2}	5.78×10^{-3}	2.23×10^{-4}

III. RESULTS AND DISCUSSION

A. Force clamp condition

Figure 2(a)(red circle) shows that the mean lifetime initially increases then decreases with external tension F; such non-monotonic variation of the lifetime represents catch-bond-like behavior of cortical dynein-MT attachment. This can be explained by the two pathways which lead to removing a motor from the MT: *i*) By breaking the motor/MT bond, or *ii*) by depolymerization of a tip subunit when a motor is bound to it. Depolymerization in the absence of a motor at the tip is much faster than the forward walking rate of a motor. Thus periods in which depolymerization is not force-dependent are negligible. Therefore detachment of motors are governed by one pathway that is enhanced by force ($k_u \sim \mathrm{e}^{F/F_d}$) and another that is suppressed by force ($\beta \sim \mathrm{e}^{-F/F_\star}$). Figure 2(a) also shows how the catch-bond behavior diminishes

with increasing characteristic depolymerization force $F_\star$. This agrees with the idea of $F_\star$ as an inverse sensitivity factor, and hence increasing $F_\star$ decreases the sensitivity of depolymerization to force, leading to purely slip bond behavior. But for low forces close to the $F = 0$ region, the dynein motors are more likely to continue their walk towards the minus end of the MT thereby stretching the elastic element and exerting a pull on the MT towards the wall. Consequently, in this regime, the tip of the MT comes closer to the wall and the depolymerization rate is enhanced by F, according to $\beta \sim e^{F/F_\star}$. So, increasing $F_\star$ increases the lifetime of the attachment by decreasing depolymerization rate.

Based on these heuristic arguments we fit the data in Fig. 2(a) with the function

$$\tau(F) = \frac{1}{\kappa(F)} = \frac{1}{k_1 e^{-\frac{F}{F_1}} + k_2 e^{\frac{F}{F_2}}} \tag{9}$$

where the best fit to the $F_\star = 0.1$ pN data (Fig. 2(a)) corresponds to $k_1 = 1.81 s^{-1}$, $F_1 \simeq 0.68 pN$ and $k_2 = 1.25 s^{-1}$, $F_2 \simeq 2.96 pN$.

We also plot the survival probability $S(t)$, the probability that till time t the MT-motor attachment survives, in the Fig:2(b) the survival probability of the MT-motor attachment is plotted for different values of external tension F. The attachment survives longer at intermediate forces (for example, at $F = 1.5$pN (blue square)) than at high and low forces. Each of the survival probabilities shown in Fig:2(b), for which F has a fixed value, has been calculated using [36, 61],

$$S(t) = \exp\Big(-\kappa(F)t\Big) \tag{10}$$

where $\kappa(F)$ is calculated using Eq.9. In the inset of Fig.2(b) the corresponding distributions of the lifetimes of the attachments are shown. Here also the distribution is broader at intermediate force $F = 1.5$pN (blue square) than at high and low forces. The lines are plotted by taking $-dS(t)/dt$ using Eq.10. At low and intermediate force region, the fitted line matches with our simulated data points but at high force, it does not match properly.

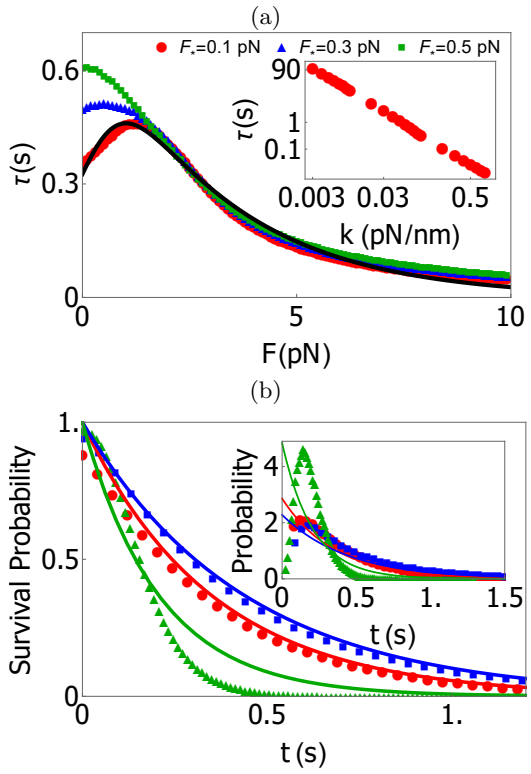

FIG. 2. (a) Mean lifetime τ of the attachment against the applied external tension F for three different $F_\star = 0.1, 0.3, 0.5$pN and fixed $N_d = 10$. The solid black line has been obtained by fitting eq.(9) to the data. Mean lifetime τ vs spring stiffness k for fixed $F = 0.1$pN is shown in the log-log plot in the inset of (a). (b) Survival probabilities are shown for three different external forces, F = 0.1pN (red circle), F = 1.5pN (blue square) and F = 4pN (green triangle). The solid lines in color have been obtained from eq.(10). In the inset of (b) the lifetime distributions are shown for the same forces; the solid lines, in corresponding colors, have been obtained by evaluating derivative of the eq.(10).

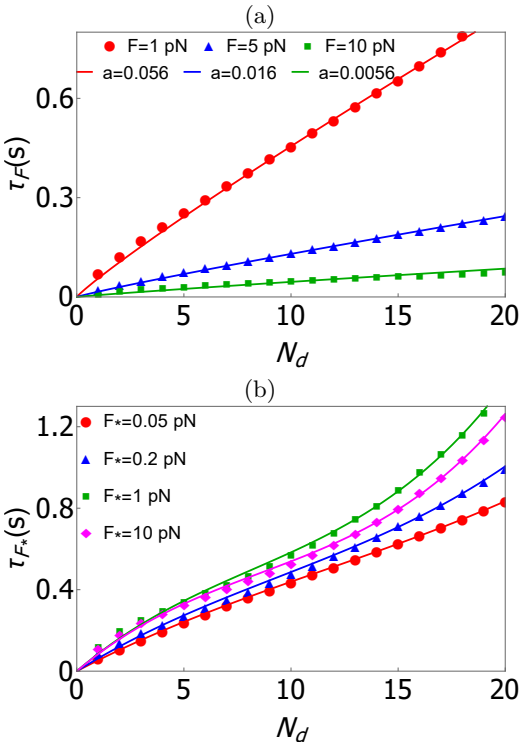

FIG. 3. (a) Mean lifetime τ of the attachment against the the number of motors N_d is shown for three different forces for $F = 1$, 5 and 10 pN keeping $F_\star = 0.1$ pN fixed (solid lines are best fits to data with eq. (11)). (b) Mean lifetime τ of the attachment against the the number of motors N_d is shown for four different $F_\star = 0.05$, 0.2, 1 and 10 pN keeping $F = 1$ pN fixed. The four solid lines in (b) have been obtained as best fits with eq. (12) for distinct sets of the parameters a, b, c given in tableII.

We generate the fitted line by substituting Eq.9 in Eq.10 but as Eq.9 does not fit properly at high force (Fig:2(a)) so the green line in Fig:2(b) deviates from simulated data points at high force.

In Fig.3 we show the dependence of the mean time τ on the total number N_d of the motors. In Fig.3(a) we plot mean time τ as a function of N_d for three different values of force F, at a fixed value $F_\star = 0.1$ pN. The data in this figure fit well with the form

$$\tau_F \propto N_d^\nu, \tag{11}$$

with the value $\nu \simeq 0.91$ of the fitting parameter ν. In Fig.3(b) we show the variation of the mean time τ with the total number N_d of the motors for four different values of the parameter $F_\star$ at a fixed force $F = 1$ pN. The data fit well with the polynomial

$$\tau_{F_\star} = aN_d - bN_d^2 + cN_d^3, \tag{12}$$

the values of all the fitting parameters a, b, c for the best fit to Eq.12 in Fig.3(b) are given in table II.

1. *Presence of catch-bond at dynein head*

In an *in vitro* experiment Kunwar et al. [62] observed catch-bond-like behavior where the unbinding rate of a single dynein motor decreases with increasing force because of a conformational change at the bounded head of the dynein motor (see also [63] and references therein). In a very recent study Nair et al. [54] proposes a threshold force bond deformation (TFBD) model to explain the catch-bond behavior of dynein. According to the TFBD model force-induced deformation of the bond between the dynein head and MT causes the catch-bond behavior [64]. The deformation energy for the ith motor is given by $E_{def}(F_i) = \phi[1 - exp(-|F_i|/f_{def})]$, where the deformation energy is given by ϕ and f_{def} is the characteristic deformation force. As the catch-bond behavior is observed [62] above a threshold force $F_i > f_m$ then according to TFBD model deformation energy is

$$E_{def}(F_i) = H(|F_i| - f_m)\phi[1 - exp(-(|F_i| - f_m)/f_{def})] \tag{13}$$

Then the effective unbinding rate is given by

$$k_u(F_i, n) = nk_{u0}e^{[-E_{def}(F_i)+|F_i|/F_d]} \tag{14}$$

To study the effect of bounded head deformation in the presence of external force, instead of using the unbinding rate given by eq.3, we have used eq.14 given by the TFBD model and calculated the mean lifetime of the attachment. In Fig.4 we have shown the mean lifetime as a function of external force. Here the maximum lifetime is 7 times larger and catch-bond like behavior becomes clearly distinguishable when compared to Fig.2(a). Here we also see that increasing $F_\star$ decreases the sensitivity of depolymerization to force but the non-monotonic variation in unbinding rate (eq.14) is responsible for the catch-bond-like behavior, even for high $F_\star$. In Fig.4 for $F_\star = 0.5$pN in the small force ($0 < F < 1.5$ pN) region, lifetime decreases slightly because of the effect of β similar to Fig.2(a). But as the F increases ($2 < F < 5$pN) the catch-bond-like behavior of unbinding rate increases the lifetime of the attachment because in that force range decreasing the unbinding rate (eq.14) enables the motors to remain bound to the MT for longer time. Around F $\simeq$ 11pN a small bump is present because of change in slope in the force in eq.14.

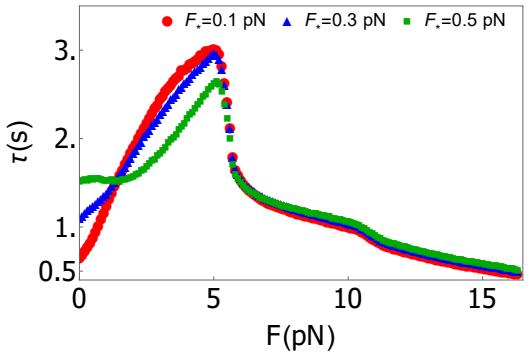

FIG. 4. Mean lifetime τ of the attachment against the applied external tension F for three different $F_\star = 0.1, 0.3, 0.5$pN and fixed $N_d = 10$ in the presence of catch-bond at the bounded dynein head. Parameters are taken from TFBD model [54] $\phi = 68\ k_BT$, $f_m = 1.4$pN and $f_{def} = 40.7$pN and rest of the parameters are given in Table:I.

B. Force ramp condition

Here we present results of our simulation under the common force spectroscopy protocol of measuring the rupture force of the attachment when increasing force with time $F(t) = rt$, and repeating over a range of loading rates, r. In Fig: 5 and Fig: 6(a) the probability distribution of rupture force $\rho(F)$ and survival probability $S(F)$ are shown for the same range of loading rates. It is important to note that at low loading rate the most probable rupture force is not zero, but instead is peaked around 0.2 pN (Fig. 5, $r = 1$ pNs^{-1}). This indicates a near-equilibrium regime in which the wall-MT attachment is stabilized by the rebinding rate k_{on}. As loading rate increases, the rupture transitions from a near-equilibrium to a kinetic regime as a second peak emerges at high rupture force and becomes prominent (Fig. 5, $r = 50$ pNs^{-1}).

The colored lines in Figs. 5 and 6(a) are the fitting of simulation data using the function [36, 61],

$$S(F) = \exp\left[-\frac{1}{r}\int_0^F \kappa(F')dF'\right] \tag{15}$$

We compare the approximation for the lifetime in Eq.9 against the simulated data through calculating the sur-

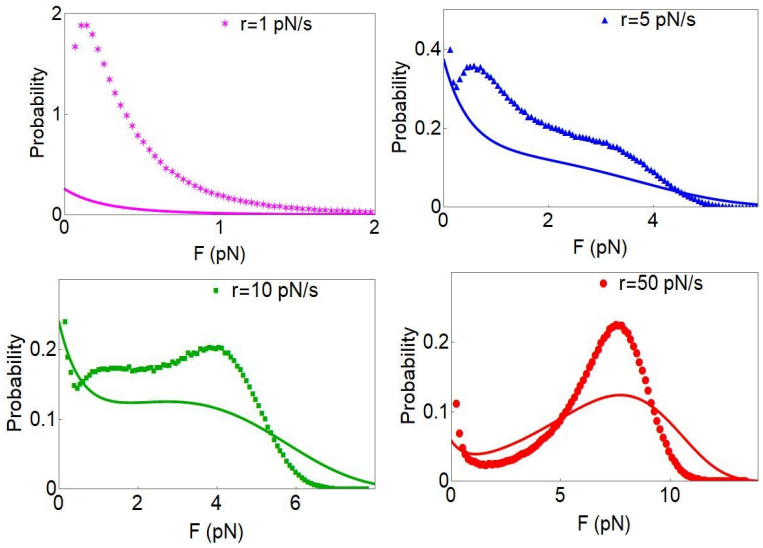

FIG. 5. Probability density of rupture force of cortical dynein-MT attachment with $N_d = 10$ are shown for four different loading rates, namely, $r = 1pNs^{-1}$ (magenta star),$r = 5pNs^{-1}$ (blue triangle), $r = 10pNs^{-1}$ (green square) and $r = 50pNs^{-1}$ (red circle) (solid lines have been obtained from Eq. (16)).

vival probability and corresponding probability distribution as [36, 61],

$$\rho(F) = -\frac{dS(F)}{dF} = \frac{\kappa(F)}{r}\exp\left[-\frac{1}{r}\int_0^F \kappa(F')dF'\right] \quad (16)$$

Equation 16 coincides with the general form of the simulated data at high forces (red line in the Fig. 5), but disagree at low forces. This can be expected since eqs. 15,16 assume a first-passage process and does not account for binding reversibility at low loading rate and low force. In the Fig. 6(a) the survival probabilities are plotted at the same loading rates for which the rupture force distributions have been shown in the Fig. 5. Here at high loading rate, $r = 50$ pNs^{-1} (red circle in Fig. 6(a)) probability of survival remain high upto a high force $F = 6$pN. But lower the loading rates survival probability drops more sharply. In the Fig. 6(b) the mean rupture force with loading rate shows the familiar behavior of a force spectrum where mean rupture force increases with increasing loading rate. In the irreversible approximation the mean rupture force, f, is given by [36, 61]

$$f = \int_0^\infty F\rho(F)dF \quad (17)$$

We substitute $\kappa(F)$ from Eq.(9) into Eq.(16) to calculate mean rupture force f from (17). We find good agreement at both low and intermediate loading rates (black line in the Fig:6(b)). At large loading rates the data becomes non-linear with log-loading rate, growing to larger rupture forces than the prediction of Eq. (17). This is likely explained by considering that faster loading rates allow less time for the dissociation and depolymerization processes to remove bound motors, ultimately leading to rupture of more motor-MT bonds.

IV. CONCLUSIONS

Extending the earlier generalizations [20] of the concept of a ligand, we have treated a microtubule (MT) as a 'ligand' that is tethered to a 'receptor' wall by a group of minus-end directed molecular motors [23]. The tails of the motors are permanently anchored on the wall while their motor heads can bind to- and unbind from the MT. This model of MT-wall attachment captures only a few key ingredients of the MT-cortex attachments in eukaryotic cells, particularly those formed during chromosome segregation. This minimal model incorporates the polymerization and depolymerization kinetics of MT. But, for the sake of simplicity, it does not include the processes of 'catastrophe' and 'rescue' that are caused by the 'dynamic instability of MT filaments [21] although these can be captured in an extended version of this model [65]. We consider a pre-formed MT-wall attachment and carry out computer simulations to study statistical properties of its rupture under conditions that mimic the protocols of force-clamp and force-ramp experiments *in-vitro* [35, 36]. The simulation results that we report are interpreted in the light of the theory of single-molecule force

spectroscopy, popularized by Bell [40] and some of its later generalizations [36].

This work is not aimed at an understanding of the mechanism of catch-/slip-bond formed by a single dynein motor head with its binding site on a MT. Instead, the phenomenon of our interest here is the *collective* dynamics of a system consisting of N_d cortex-anchored dyneins that bind to-/unbind from- the plus-end region of a single MT. The non-monotonic variation of the lifetime of the entire attachment system is its *emergent collective mechanical property* which can be interpreted as a catch-bond. The data presented in Fig.2(a) unambiguously establish this collective catch-bond-like emergent behaviour even when none of the dyneins individually possesses a catch-bond at its MT-binding head. A comparison of Fig.2(a) with Fig.4 also shows that the collective lifetime of the attachment merely becomes longer if the MT-binding head of each individual dynein has a catch-bond. The nontrivial dependence of these collective properties on the number N_d of the dyneins are shown by the data in Fig.3 (and also some related data in Fig.6).

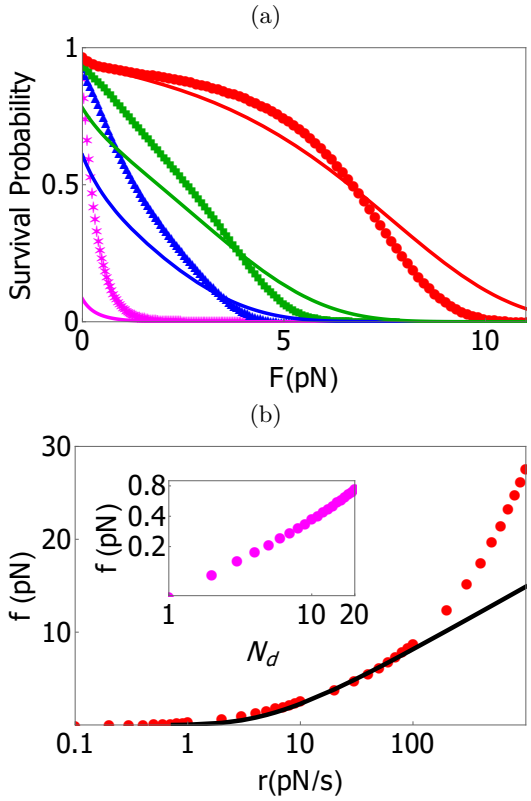

FIG. 6. (a) Survival probability for different loading rates; same symbols in Fig: 5 and (a) correspond to same set of parameters values. (solid lines are from Eq. (15)) (b) Mean rupture force for fixed $N_d = 10$ is plotted against loading rate in a logarithmic scale. The dependence of the mean rupture force f on the number of motors N_d for fixed loading rate $r = 1pNs^{-1}$ is displayed as log-log in the inset (magenta circles). The black solid line has been obtained evaluating the right hand side of Eq. (17)) by numerical integration.

TABLE III. Experimentally measurable quantities

Protocols	Measurable quantity
Force Clamp F=Clamped force	Distribution of lifetimes at different F Variation of mean lifetime with F Survival probability at different F Variation of mean lifetime with N_d
Force Ramp r = Loading rate	Distribution of rupture forces at different r Variation of mean rupture force with r Survival probability at different r Variation of mean rupture force with N_d

The quantities that we have computed are listed in the table III; in principle, these quantities can be measured, in molecular force spectroscopic measurements *in-vitro*. *In-vitro* experiments have been designed which remarkably resemble the conceptual model depicted in Fig.1(a), albeit without application of a controlled force. Laan et al. [11] used a microfabricated vertical barrier that mimics the cell cortex. Dynein motors were anchored on the barrier and captured the MT that grew from a centrosome which was fixed on a horizontal glass surface. A slightly different experimental set up was used by Hendricks et al. [66] in which a dynein coated bead was used to mimic the cell cortex. These authors demonstrated the stabilization of the MT within the broader context of the role of MT-cortex interaction in positioning of the mitotic spindle [11, 66]. However, the possibility of controlling the force on the MT by an Atomic Force Microscope or Optical Trap should motivate extending these experimental setups to test the results of our theoretical model in the near future.

The phenomenon of "bond rupture" studied here can be viewed from a broader perspective because of its close relation with many other similar phenomena. Both thermally activated (spontaneous) and force induced peeling off, or depinning of, a filament bound to another filament or to a surface by weak non-covalent bond or by passive linker molecules have been studied extensively in the last two decades [67–72]. In more recent times, the forced peeling of a filament tethered to a surface by active linkers (e.g., a MT tethered to a surface by dynein motors) have begun to receive attention [73]. This system is also analogous to *in-vitro* gliding assays where MTs glide by the action of the strokes of ATP-consuming motors that have their tail end immobilized on a flat surface. In the latter situation, in the absence of external force, the filament glides remaining approximately parallel to the surface. In contrast, in our model, the motors make end-on attachment with the MT that is oriented perpendicular to the surface on which the tail ends of the motors are immobilized. However, often the plus end of the astral MTs bend whereby a segment of it makes lateral contact with the cortex linked by the dynein motors. This bent segment, which is similar to the MTs in a gliding assay, can be incorporated in an extended version of our model in near future.

By analyzing a simple theoretical model *in-silico*, using the protocols of MFS, we elucidate a mechanism by which the strength and stability of MT-cortex attachment, that emerge as collective emergent properties, can be regulated by external tension. Our analysis confirms that the competing kinetics of polymerization and depolymerization of MTs, coupled with force-induced strong suppression of depolymerization rate, leads to overall lifetimes of the attachments that show a non-monotonic behavior akin to catch-bonds. The same force-induced suppression of MT depolymerization is also known to give rise to the catch-bond-like behavior of MT-kinetochore attachments [74]. Thus, our work here reveals that a common mechanism (namely, tension-induced suppression of MT depolymerization) can give rise to catch-bond-like collective behavior of two altogether different types of attachments, in spite of all the differences between their composition, structure and dynamics. Therefore, our work, reported here, should motivate MFS of other molecular joints formed by MTs, in search of possible occurrence of similar catch-bond-like phenomena in even more diverse systems. Our observations also strongly suggest that the tension-induced suppression of MT depolymerization may be an important aspect of Nature's principle of design of multi-component molecular machineries. Examining this possibility in the broader context of molecular evolution of the MT-based machineries for chromosome segregation [76–80] will also throw light on Nature's principles of evolutionary design.

ACKNOWLEDGMENTS

DC thanks Gaurav Arya for valuable comments on an earlier preliminary version of the work. This work has been supported by a J.C. Bose National Fellowship (DC) and by the "Prof. S. Sampath Chair" Professorship (DC). Sandia National Laboratories is a multimission laboratory managed and operated by National Technology and Engineering Solutions of Sandia, LLC., a wholly owned subsidiary of Honeywell International, Inc., for the U.S. Department of Energy's National Nuclear Security Administration under contract DE-NA-0003525. The authors also thank the anonymous referees for many useful detailed comments and suggestions that have helped in significant improvement of the paper.

Appendix A: Master equations for the kinetics

The probability that (the midpoint of) a motor is located at x_{mi} and MT tip is at x_M, while the total number $n(t)$ of motors are bound to the MT simultaneously at that instant of time, is given by $P_n(x_{mi}, x_M, t)$. Velocity of whole MT body is given by v_F. Note that x_M is a continuous variable whereas n can take only non-negative integer values. Let $P(y_m|\underline{x_{mi}})$ be the conditional probability that, given a MT-bound motor located at site x_{mi}, there is another MT-bound motor at site y_m on the MT ($x_M < x_{mi}, y_m$). Then $\xi(y_m|\underline{x_{mi}}) = 1 - P(y_m|\underline{x_{mi}})$ is the conditional probability that, given a motor at site x_{mi}, the site y_m is empty. Let $\xi(x_{mi})$ be the probability that site x_{mi} is not occupied by any motor, irrespective of the state of occupation of any other site.

Under mean field approximation (MFA), the equations governing the time evolution of $P_n(x_{mi}, x_M t)$ is given by

$$\begin{aligned}\frac{dP_n(x_{mi},x_M,t)}{dt} = &\underbrace{k_f(F_i)P_n(x_{mi}-\delta,x_M,t)\xi(x_{mi}|\underline{x_{mi}-\delta}) - k_f(F_i)P_n(x_{mi},x_M,t)\xi(x_{mi}+\delta|\underline{x_{mi}})}_{\text{Forward stepping of the motor if target site is empty}}\\ &+\underbrace{k_r(F_i)P_n(x_{mi}+\delta,x_M,t)\xi(x_{mi}|\underline{x_{mi}+\delta}) - k_r(F_i)P_n(x_{mi},x_M,t)\xi(x_{mi}-\delta|\underline{x_{mi}})}_{\text{Reverse stepping of the motor if target site is empty}}\\ &+\underbrace{k_{on}(n-1)(1-P_{n-1}(x_{mi},x_M,t)) - k_{on}(n)(1-P_n(x_{mi},x_M,t))}_{\text{Binding of motor to an empty site on MT}}\\ &+\underbrace{k_u(F_i,n+1)P_{n+1}(x_{mi},x_M,t) - k_u(F_i,n)P_n(x_{mi},x_M,t)}_{\text{Unbinding of motor from an occupied site on MT}} - \underbrace{v_F\frac{\partial P_n(x_{mi},x_M,t)}{\partial x_M}}_{\text{Drift velocity of whole MT body}}\end{aligned} \tag{A1}$$

where

$$v_F = \frac{F - \sum_{i=1}^{n} F_i(x_{mi})}{\Gamma} \tag{A2}$$

[1] J. R. McIntosh, M. I. Molodotsov and F. I. Ataullakhanov, Quart. Rev. Biophys. **45**, 147 (2012).
[2] D. C. Bouck, A. P. Joglekar and K. S. Bloom, Annu. Rev. Genet. **42**, 13.1 (2008).
[3] K. J. Helmke, R. Heald and J. D. Wilbur, Int. Rev. Cell Mol. Biol. **306**, 83 (2013).
[4] S. Petry, Annu. Rev. Biochem. **85**, 659 (2016).
[5] T. M. Kapoor, Biology. **6**, 8 (2017).
[6] I. M. Cheeseman and A. Desai, Nat. Rev. Mol. Cell. Biol. **9**, 33 (2008).
[7] P. DeWulf, W. C. Earnshaw, (Eds.) *The Kinetochore: From Molecular Discoveries to Cancer Therapy*, (Springer 2009).
[8] C. L. Asbury, Biology. **6**, 15 (2017).
[9] J. M. Scholey, G. Civelekoglu-Scholey, and I. Brust-mascher, Biology. **5**, 15 (2016).
[10] C. Kozlowski, M. Srayko and F. Nedelec, Cell **129**, 499 (2007).
[11] L. Laan, S. Roth, M. Dogterom, Cell Cycle. **11**, 3750 (2012).
[12] S. Kotak, and P. Gönczy, Curr. Opin. Cell Biol. **25**, 741 (2013).
[13] M. S. Lu, and C. A. Johnston, Development **140**, 1843 (2013).
[14] F. J. McNally, J. Cell Biol. **200**, 131 (2013).
[15] F. di Pietro, A. Echard, X. Morin, EMBO Rep. **17**, 1106 (2016).
[16] S.W. Grill, K. Kruse and F. Jülicher, Phys. Rev. Lett. **94**, 108104 (2005).
[17] J. Pecreaux, J.C. Röper, K. Kruse, F. Jülicher, A.A. Hyman, S.W. Grill and J. Howard, Curr. Biol. **16**, 2111 (2006).
[18] E. A. Evans and D. A. Calderwood, Science, **316**, 1148 (2007).
[19] P. Bongrand, Rep. Prog. Phys. **62**, 921 (1999).
[20] M. Karplus, J. Mol. Recognit. **23**, 102 (2010).
[21] A. Desai and T.J. Mitchison, Annu. Rev. Cell Dev. Biol. **13**, 83 (1997).
[22] R. T. McLaughlin, M. R. Diehl and A. B. Kolomeisky, Soft Matter. **12**, 14 (2016).
[23] D. Chowdhury, Phys. Rep. **529**, 1 (2013).
[24] A. B. Kolomeisky, *Motor proteins and Molecular Motors*, (CRC Press, 2015).
[25] N. Tamura and V. M. Draviam, Open Biol. **2**, 120132 (2012).
[26] R. H. Wade, Mol. Biotechnol. **43**, 177 (2009).
[27] A. Akhmanova, M. O. Steinmetz, Nat. Rev. Mol. Cell Biol. **16**, 711 (2015).
[28] M. Vleugel, M. Kok and M. Dogterom, Cell Adhesion & Migrartion **10**, 475 (2016).
[29] H. Tuncay and K. Ebnet, Cell. Mol. Life Sci. **73**, 1195 (2016).
[30] H. Bowne-Anderson, M. Zanic, M. Kauer and J. Howard, Bioessays **35**, 452 (2013).
[31] B. Govindan and W.B. Spillman, Jr. Phys. Rev. E **70**, 032901 (2004).
[32] M. Ebbinghaus and L. Santen, Biophys. J. **100**, 832 (2011).
[33] M. Zeitz and J. Kierfeld, Biophys. J. **107**, 2860 (2014).
[34] J. Rickman, C. Duellberg, N.I. Cade, L.D. Griffin and T.Surray, PNAS **114**, 3427 (2017).
[35] A.R. Bizzarri and S. Cannistraro (eds.) *Dynamic Force Spectroscopy and Biomolecular Recognition*, (CRC Press, 2012).
[36] G. Arya, Molecular Simulation, **42**, 1102 (2016).
[37] D.E. Makarov, *Single Molecule Science* (CRC Press, 2015).
[38] D.E. Makarov, J. Chem. Phys. **144**, 030901 (2016).
[39] M. Muller, S. Klumpp, and R Lipowsky, PNAS. **105**, 4609, (2008).
[40] G.I. Bell. Science, **200**, 618, (1978).
[41] H.A. Kramers. Physica, **7**, 284,(1940).
[42] R. Mallik, B.C. Carter, S.A. Lex, S.J. King, and S.P. Gross. Nature, **427**, 649, (2004).
[43] S.L. Reck-Peterson, A. Yildiz, A.P. Carter, A. Gennerich, N. Zhang, and R.D. Vale. Cell, **126**, 335, (2006).
[44] S. Toba, T.M. Watanabe, L. Yamaguchi-Okimoto, Y.Y. Toyoshima, and H. Higuchi. Proc. Natl. Acad. Sci. USA, **103**, 5741, (2006).
[45] A. D. Franck, A. F. Powers, D. R. Gestaut, T. Gonen, T. N. Davis, C. L. Asbury, Nat Cell Biol **9**, 832 (2007).
[46] A. P. Joglekar and A.J. Hunt, Biophys. J. **83**, 42 (2002).
[47] T. Hill, Proc. Natl. Acad. Sci. U.S.A. **82**, 4404 (1985).
[48] B. Shtylla and J. P. Keener, SIAM J. Appl. Math. **71**, 1821 (2011).
[49] J. C. Waters, T.J. Mitchison, C.L. Rieder and E. D. Salmon, Mol. Biol. Cell. **7**, 1547 (1996).
[50] S. J. King, T. A. Schroer, Nat. Cell. Biol. **2**, 20 (2000).
[51] S. L. Reck-Peterson, A. Yildiz, A. P. Carter, A. Gennerich, N. Zhang, R. D. Vale, Cell. **126**, 335 (2006).
[52] R. Mallik, D. Petrov, S. A. Lex, S. J. King, S. P. Gross, Nature **427**, 649 (2005).
[53] M. Nishiura, T. Kon, K. Shiroguchi, R. Ohkura, T. Shima, Y. Y. Toyoshima, K. Sutoh, J. Biol.Chem. **22**, 22799 (2004).
[54] A. Nair, S. Chandel, M. K. Mitra, S. Muhuri, and A. Chaudhuri, Phy. Rev. E. **94**, 032403 (2016).
[55] W. F. Marshall, J. F. Marko, D. A. Agard and J. W. Sedat, Curr. Biol. **11**, 569 (2001).
[56] D.T. Gillespie, Annu. Rev. Phys. Chem. **58**, 35(2007).
[57] S. Redner, *A Guide to First-Passage Processes* (Cambridge University Press, Cambridge, 2001)
[58] S. Redner, R. Metzler and G. Oshanin, (eds) *First-passage Phenomena and their Applications*, (World Scientific Publishing Co., 2014).
[59] S. Iyer-Biswas and A. Zilman, Adv. Chem. Phys. **160**, 261 (2016).
[60] N. Polizzi, M.J. Therien, D.N. Beratan, Israel J. Chem. **56**, 816 (2016).
[61] R. W. Friddle, in: [35].
[62] A. Kunwar, S. K. Tripathy, J. Xu, M. K. Mattson, P. Anand, R. Sigua, M. Vershinin, R. J. McKenneye, C. C. Yu, A. Mogilner, and S. P. Gross, PNAS **108**, 18960 (2011).
[63] R. Mallik, A.K. Rai, P. Barak, A. Rai and A. Kunwar, Trends in Cell Biol. **23**, 575 (2013).
[64] Y. V. Pereverzev and O. V. Prezhdo, Phys. Rev. E. **73**, 050902 (2006).
[65] D. Ghanti, Ph.D. Thesis, IIT Kanpur (2018).
[66] A.G. Hendricks, J.E. Lazarus, E. Perlson, M.K. Gardner, D.J. Odde, Y.E. Goldman and E.L.F. Holzbaur, Curr. Biol. **22**, 632 (2012).

[67] M. Aliee and A. Najafi, Phys. Rev. E **78**, 051802 (2008).
[68] P. benetatos and E. Frey, Phys. Rev. E **67**, 051108 (2003).
[69] J. Kierfeld, T. Kühne and R. Lipowsky, Phys. Rev. Lett. **95**, 038102 (2005).
[70] X. Oyharcabal and T. Frisch, Phys. Rev. E **71**, 036611 (2005).
[71] D.B. Staple, M. Geisler, T. Hugel, L. Kreplak and H.J. Kreuzer, New J. Phys. **13**, 013025 (2011).
[72] R. Borah and P. Debnath, Soft Matter **12**, 4406 (2016).
[73] A. Chaudhuri and D. Chaudhuri, Soft Matter **12**, 2157 (2016).
[74] A. K. Sharma, B. Shtylla and D. Chowdhury, Phys. Biol.**11**, 036004 (2014).
[75] D. Ghanti, S. Patra and D. Chowdhury, Phys. Rev. E **97**, 052414 (2018).
[76] I.B. Heath, Int. Rev. Cytology **64**, 1 (1980).
[77] A.C. Schmit and P. Nick, Plant Cell Monogr. **11**, 233 (2008).
[78] B. Akiyoshi and K. Gull, Open Biol. **3**, 130023 (2013).
[79] H. Drechsler and A.D. McAinsh, Open Biol. **2**, 120140 (2012).
[80] J.R. McIntosh et al. J. Cell Biol. **200**, 459 (2013).